Second International Symposium on Marine Propulsors
smp'11, Hamburg, Germany, June 2011

RANSE Code Application for Ducted and Endplate Propellers in Open Water

Henri Haimov, Jorge Vicario, Javier Del Corral

Canal de Experiencias Hidrodinámicas de El Pardo (CEHIPAR), Madrid, Spain

ABSTRACT

This paper reflects the application of the commercial RANSE code ANSYS-CFX® and its mesh generator ICEM® to two types of propulsors in a range of open water non-cavitating conditions. The mesh dependence and convergence of the results are presented. The validation is carried out using open water model experimental data. The numerical prediction for both propulsors is able to reproduce the experiment very well in a practical range of advances. For propeller in duct 37, a comparison is also done with pressure measurements on the inner side of the nozzle. Propeller in nozzle 19A was also calculated in full scale. It was confirmed that the resulting total thrust is practically not affected by the scale, while the forces on the duct and the propeller are. For the endplate CLT propeller the influence of the turbulence model (SST and k-ε) has been also evaluated. The combined effect of Reynolds number and loading on the thrust and torque has been obtained by comparing model and full scale calculations in turbulent flow, confirming the peculiarities of the ducted propellers and the substantial gain of efficiency for the CLT propeller. Comparing with the extrapolation method currently applied, it is concluded that further use of RANSE code may permit to improve it.

Keywords

Propeller in nozzle, CLT propeller, CFD, RANSE, Scale effect

1 INTRODUCTION

Nowadays, most of the ships are fitted with conventional propellers due to their relative simplicity, wide speed range of acceptable efficiency, and the advances in the design procedures permitting to take into account criteria like noise and vibrations (N&V) excitation, which has been an issue of increased concern. Nevertheless, a frequent consequence of less excitation is the reduction of open water efficiency, especially at high loading conditions. The present work is dedicated to two types of "non-conventional" propulsors that, in certain conditions, have shown to improve the efficiency with respect to conventional propeller. Although the propeller in nozzle, called also ducted propeller, can now be considered a conventional propulsor, its peculiarities still create difficulties to the precision of its full scale hydrodynamic performance prediction and continues to be of interest for the research community, as can be seen from recent publications given in the References.

In order to validate the use the RANSE code, two test examples of ducted propellers, corresponding to different nozzles, have been calculated. The first one is a case of set of open water and pressure measurements on the inner side of the duct carried out at atmospheric conditions in the depressurized towing tank at MARIN (Falcao de Campos 1983) with the nozzle 37 and a Kaplan type CP propeller. Case 2 is a 249 TDW fishing vessel fitted with propeller in nozzle 19A and a similar to K_a-series FPP, designed and tested in CEHIPAR (Bobo 2005). Detailed geometry of the propulsors and approximate open water setup have been reproduced and used to compute the performance in a range of advances.

The endplate propellers, especially in its modality, called loaded tip propellers (CLT) (Pérez Gómez & González-Adalid 1995), are extending their application for wide types of ships due to benefits in efficiency and vibration excitation found in full scale conditions (Gennaro et al 2009). The need of reliable tools for prediction of the performance of such propellers is obvious, but only few of the existing inviscid codes are able to treat the peculiar geometry of the blades, and additionally, there are evidences that viscous effects play an important role. An application of RANSE solver for a CLT propeller is reported in Sánchez-Caja et al (2006), showing its applicability and the need of more contributions to answer the variety of issues of this complicated propulsor.

2 RANSE, MESHING AND CAD CODES USED

The CFD code applied is ANSYS CFX®, v.12 (ANSYS 2009) with the meshing tool ICEM®. The Reynolds Averaged Navier-Stokes equations are solved numerically by a finite volume technique.

3D CAD models of the propulsors have been generated starting from the classical profile description of the propellers blades and the nozzles. The corresponding IGES files are submitted to the meshing program. Additional effort is necessary for the description of the CLT propellers as the endplates have to be aligned to the

flow and thus, intersects with the blade tip area on variable radial sections. Recently we use the CAD/CAM commercial code SolidWorks®, starting from full offsets of Cartesian points representing the detailed geometry and generated by an indoor geometric program.

The computational domain consists of an internal rotating cylinder of radius 1.5D containing the propeller and an external stationary cylinder with radius 2.5D where, in the case of the ducted propeller, the axisymmetric nozzle is located. The inlet uniform boundary condition is located at 3 to 4D upstream of the propeller plane and the constant pressure condition is imposed 4-6D downstream.

From the positive experience of free running conventional propellers (Haimov et al 2007) and considerations of the flow in different regions around the propulsors, first a basic non-structured mesh has been established (Grid_1), consisting mostly of tetrahedral elements and layers of prisms around the hard surfaces. For the ducted propeller the mesh is refined around the leading and trailing edges of the nozzle and the blades, as well as in the gap between the blade tip and the inner surface of the nozzle (Fig.1). In the case of the CLT propeller, a denser mesh is generated around and on the endplate as well. A few more meshes of increasing resolution have been also generated.

In the present study, which is dedicated to axial open water (uniform) flow, the mesh is created only in a sector corresponding to one blade of the propeller, taking advantage of the axial symmetry of the geometry and the flow. Periodic boundary condition is applied to consider the interaction with the rest of the propulsor's geometry and the smooth wall option is used in all computations.

3 DUCTED PROPELLERS

3.1 Case 1: Duct 37 with propeller 4902MARIN

The main characteristics of the propulsor and open water test conditions are given in the Tables 1, 2 and 3 below:

Table 1: Propeller overall data

Propeller – Controllable pitch	4902_MARIN
Diameter	290.0 mm
Number of blades	4
Blade area ratio	0.528
Mean pitch ratio	1.065
Boss ratio	0.307
Chord length ratio (c/D)	0.335 at $0.7R_p$

Table 2: Nozzle overall data

Profile of the contour	Duct 37
Length/Diameter ratio	0.5
Propeller tip clearance	0.7% R_p

Table 3: Open water test conditions

J	0.203	0.300	0.405	0.500	0.617
CTH	16.38	7.10	3.52	2.07	1.06

The number of grid cells in a sector, from coarse to fine, are given in Table 4.

Figure 2 is a typical graph of the forces' convergence with the iterations of the runs.

Figures 3 to 5 show the mesh dependence of the forces. The position "5" on the abscissa corresponds to the experimental value taken from the model open water test.

Table 4: Mesh statistics of Case 1

Mesh	*Elements in sector*
Grid_1	3.79E+06
Grid_2	5.82E+06
Grid_3	6.04E+06
Grid_4	6.47E+06

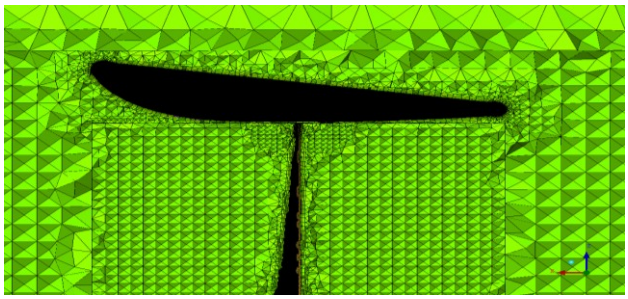

Figure 1: Mesh around the ducted propeller.

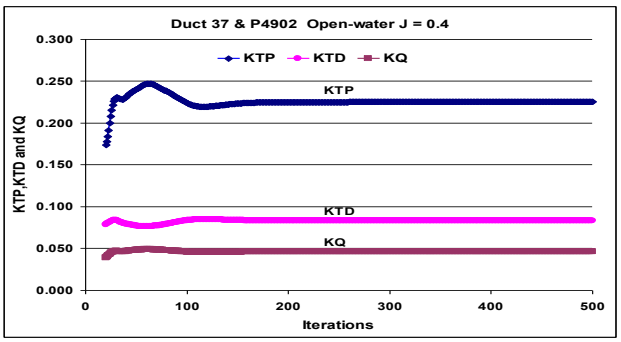

Figure 2: Convergence of forces with iterations, Case 1.

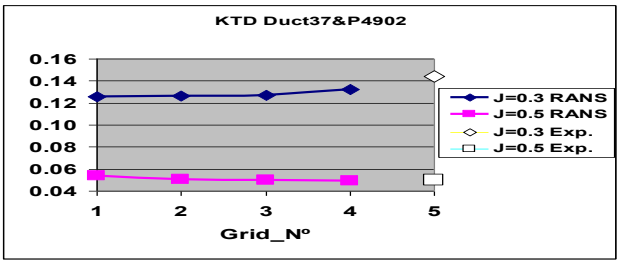

Figure 3: Convergence of duct thrust coefficient, Case 1.

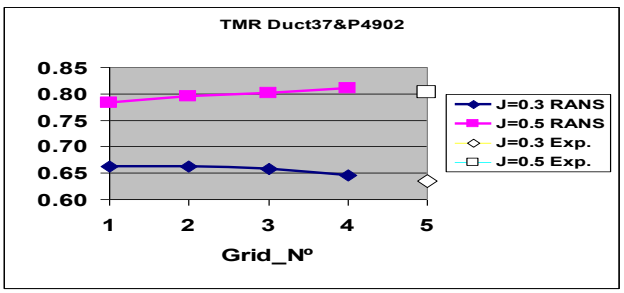

Figure 4: Convergence of thrust ratio, Case 1.

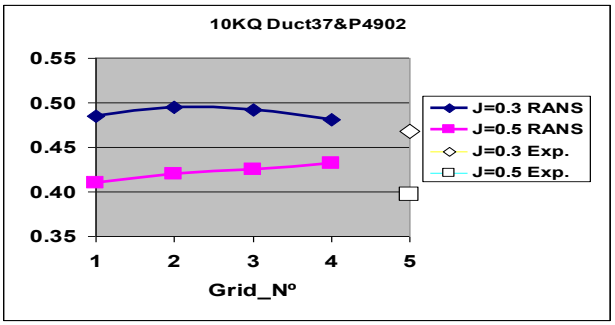

Figure 5: Convergence of the torque coefficient, Case 1.

A comparison of computed and measured open water characteristics is given in Figure 6:

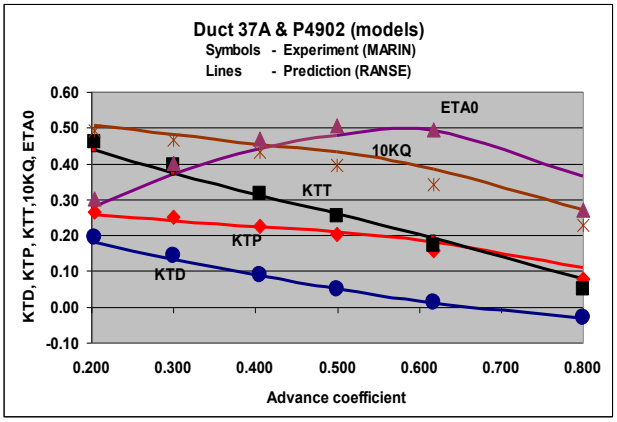

Figure 6: Open water characteristics of the propulsor.Grid4

The relative deviations are shown in Figures 7 to 9.

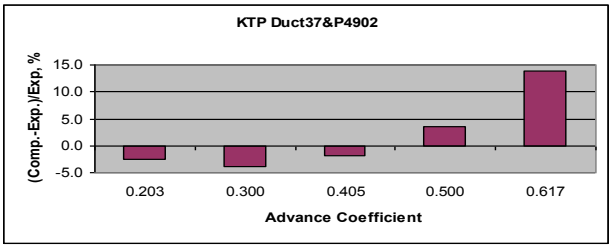

Figure 7: Validation of the propeller thrust coefficient.

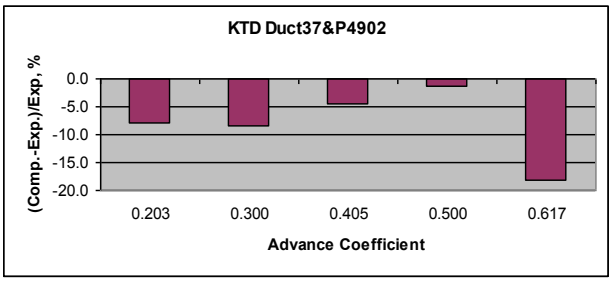

Figure 8: Validation of the duct thrust coefficient, Case 1.

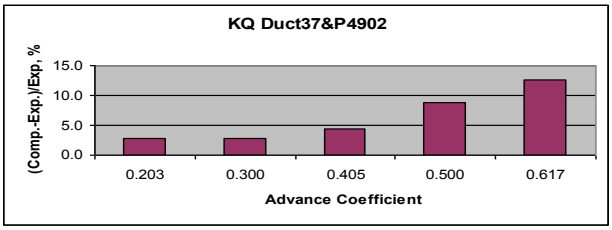

Figure 9: Validation of the propeller torque, Case 1.

The measurement (Falcao de Campos 1983) at MARIN of the pressure on locations of the nozzle inner surface for three advances has been used to compare the computations. The corresponding test conditions Reynolds numbers are shown in Table 5 below:

Table 5: Test conditions for the pressure test

J	0.203	0.405	0.617
RNP	4.55E+05	4.60E+05	4.70E+05
RND	6.24E+04	1.24E+05	1.90E+05

As practiced in the test, the angular velocity of the propeller is kept constant, varying the speed of advance. For the sake of comparison the computed pressure is presented in the same non-dimensional form as in Baltazar & Falcao de Campos (2009) in Figures 10-12:

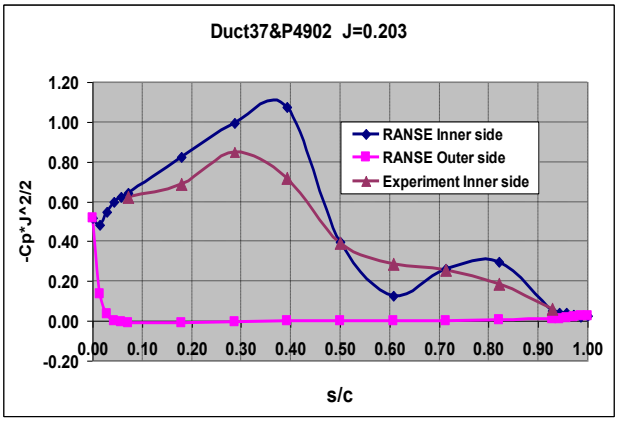

Figure10: Mean pressure on inner surface of nozzle, J=0.203.

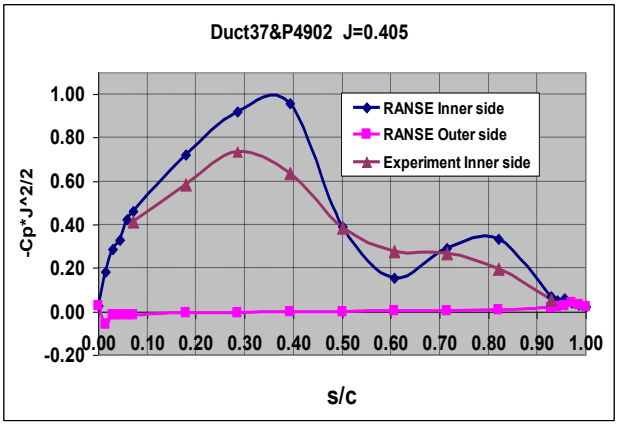

Figure11: Mean pressure on inner surface of nozzle, J=0.405.

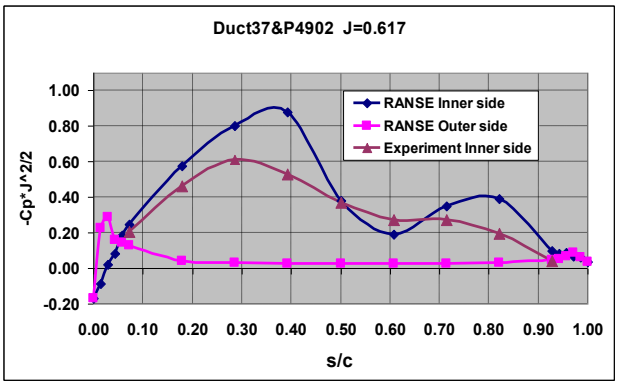

Figure12: Mean pressure on inner surface of nozzle, J=0.617.

No significant mesh dependence of the pressure was found, as can be seen in Figure 13.

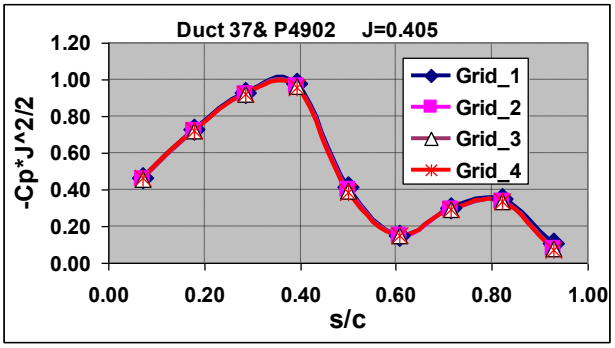

Figure 13: Convergence of the pressure on the duct.

3.2 Case 2: Duct 19A with propeller 2397CEH

The main characteristics of the propulsor and the test and calculation conditions are given in Tables 6, 7 and 8.

Table 6: Propeller overall data

Propeller – Fixed pitch	2397CEHIPAR
Diameter	251.8 mm
Number of blades	4
Blade area ratio	0.600
Mean pitch ratio	1.143
Boss ratio	0.170
Chord length ratio (c/D)	0.313 at 0.7R_p

Table 7: Nozzle overall data

Profile of the contour	Duct 19A
Length/Diameter ratio	0.5
Propeller tip clearance	0.7% R_p

Table 8: Open water test conditions

J	CTH	RNP	RND
0.20	20.0	5.00E+05	7.23E+04
0.30	8.5	5.02E+05	1.08E+05
0.40	4.5	5.06E+05	1.45E+05
0.50	2.7	5.10E+05	1.81E+05
0.60	1.7	5.15E+05	2.17E+05

The computational domain and meshing are similar to Case 1. The meshes have the following number of cells:

Table 9: Mesh statistics of Case 2

Mesh	Elements in sector
Grid_1	1.89E+06
Grid_2	5.74E+06
Grid_3	1.52E+07

The mesh dependence of the forces (not shown) has similar trends as in the previous case.

The comparison of the calculated forces with open water test results (Bobo et al 2005) is shown in Fig. 14 to 17 below. The computed averaged pressure distribution on both sides of the nozzle, for J=0.4, is presented in Fig.18.

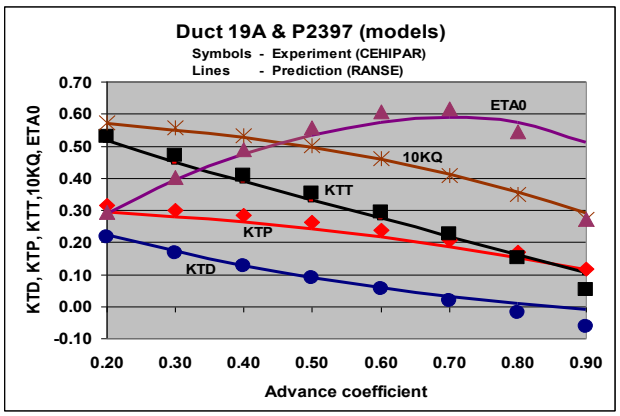

Figure 14: Open water characteristics of the propulsor.

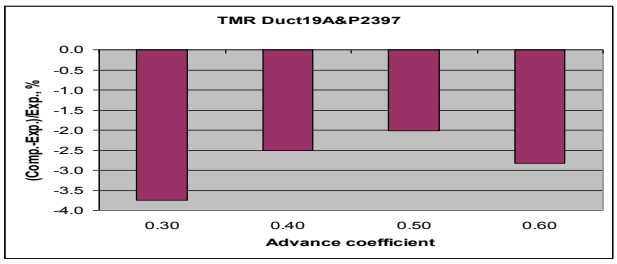

Figure 15: Validation of the thrust ratio, Case 2.

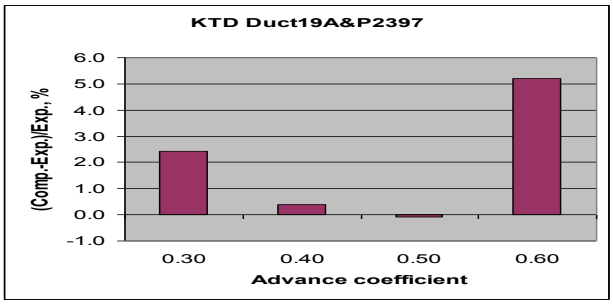

Figure 16: Validation of the duct thrust coefficient, Case 2.

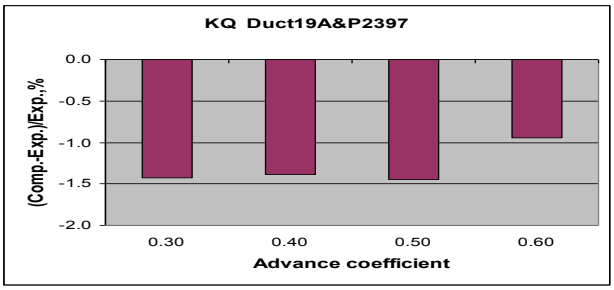

Figure 17: Validation of the propeller torque, Case 2.

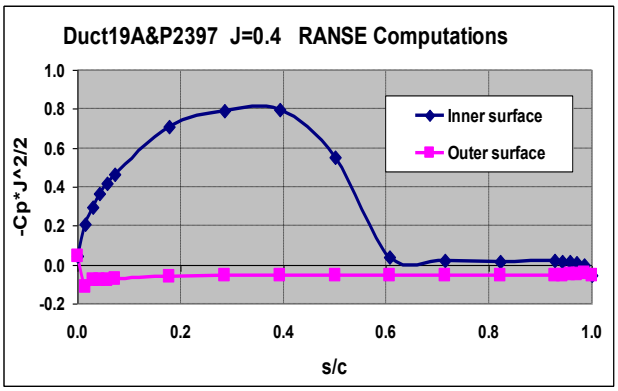

Figure 18: Mean pressure on both surfaces of nozzle, Case 2.

3.3 Scale effect for ducted propeller Case 2

The full scale conditions of the real ship used in the computations correspond to the model Case 2 scaled by factor 6.75 (diameter of the propeller 1.7m) and revolutions modeled by Froude similarity. The Reynolds number then increases more than an order of magnitude. For J=0.4 RNP=8.9E+06, and RND=2.5E+06. The convergence of the forces with the resolution of the mesh has principally been found to not be different from the model case.

Figure 19 shows the effect of Reynolds number scaling on the forces and the efficiency, presented as the relative deviation $\Delta K=(K_S-K_M)/K_M$ in % of the full scale results from the model ones.

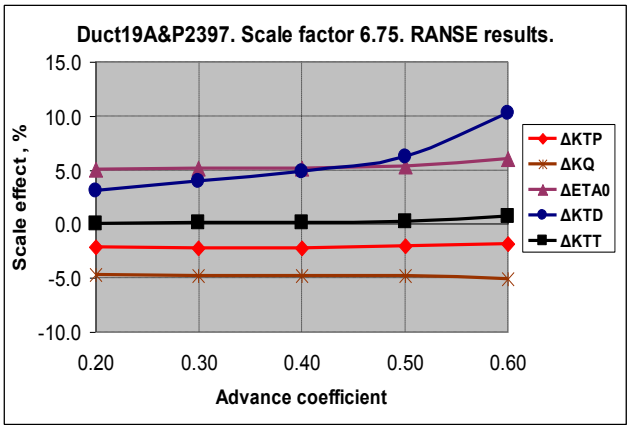

Figure 19: Scale effect on open water of ducted propeller.

3.4 Discussion

Although a clear convergence of the computational results has not been reached, the tendency is towards the experimental values, except for the torque at high advances, as can be seen in Figures 3 - 5.

Very good agreement between predictions and experiment is obtained for all forces (Figures 6-9 and 14-17) at low and moderate advances. The thrust ratio is predicted within 3.5%. The decrease of precision at high advances, corresponding to light loadings, may be associated with the small magnitude of the forces and possible separation of the flow requiring higher resolution to be detected.

The computed pressure distribution inside the nozzle (Figures 10-12) is still far from the experimental values, but substantially improves the inviscid results (Baltazar & Falcao de Campos 2009), especially in the downstream part of the duct. It is to be noted that the reverse gradient of the pressure obtained by both the present RANSE and the inviscid computations in the zone 0.6<s/c<0.8 is not observed in the experimental results. As shown in Figure 13, the pressure distribution is almost independent of the grid size, probably due to the good approach obtained even with the coarser grid.

The comparison of Figures 11 and 18, corresponding to similar thrust loading of the propeller is an example how the shape of the duct affects the pressure distribution.

The results for the scale effect shown in Figure 19 coincide within 2% with interpolation for the same scale factor and range of loadings reported in Abdel-Maksoud & Heinke (2002), although the range of Reynolds numbers is not exactly the same. Even for moderate scale factor and corresponding variation of Reynolds number from 1.5E+05 to 2.5E+06, the effect is not negligible and more pronounced for the thrust of the duct and the torque of the propeller. For moderate loadings the scaling factor results practically independent of the loading. The opposite impact of the scale on the thrust of the duct and of the propeller makes the total thrust almost independent of the scale for a practical range of advances.

4 ENDPLATE CLT PROPELLER

The CLT propeller subject to RANSE computations is the actual propulsor of a 14500 kW twin screw ROPAX ship that substituted the original high screw propellers, solving vibration problems and gaining propulsive efficiency as demonstrated by ship trials.

4.1 Model propeller RP-1-ACC_CLT1

Particulars of the propeller, designated as RP-1-ACC_CLT1 in accordance with the European project SILENV, are given in Table 10. A 3D view of the right handed propeller is shown in Figure 20.

Table 10: Propeller overall data

Propeller – Controllable pitch	RP-1-ACC_CLT1
Diameter	243.2 mm
Number of blades	4
Blade area ratio	0.520
Mean pitch ratio	1.102
Boss ratio	0.324
Chord length ratio (c/D)	0.339 at $0.7R_p$
Scale factor	17.96

Three volumetric meshes of increasing number of cells (Table 11) have been generated for a sector corresponding to one blade and $1/4^{th}$ of the hub and cap.

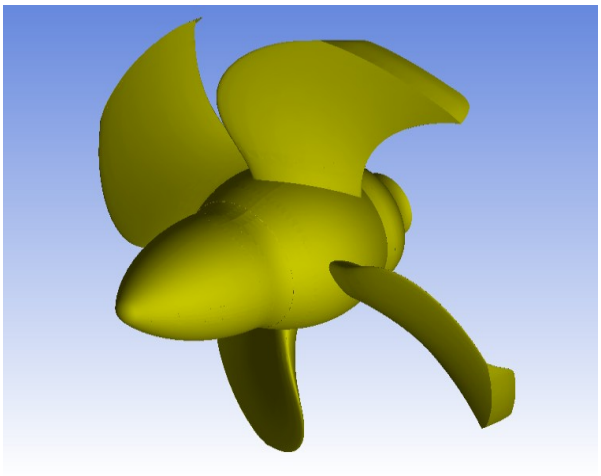

Figure 20: 3D CAD view of the CLT propeller.

Table 11: Statistics of the mesh for CLT propeller

Mesh	*Elements in sector*
Grid_1	2.0E+06
Grid_2	5.1E+06
Grid_3	7.5E+06

A detail of the medium grid around the blade tip and the endplate is shown in Figure 21 below.

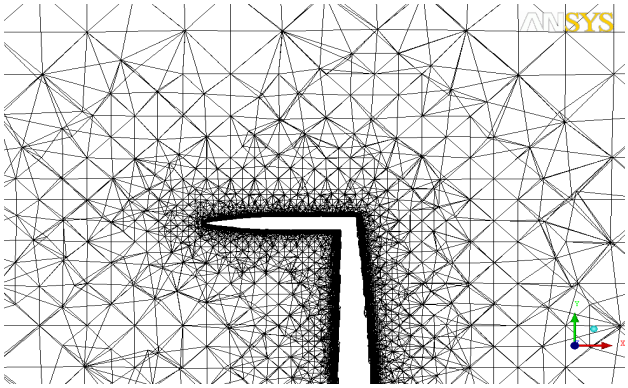

Figure 21: Detail of the mesh at the tip of the blade.

The open water computations have been carried out for a practical range of advances of available experimental data. The Reynolds number RNP varies from 8.9E+05 to 9.7E+05. Figure 22 shows the comparison between computed and measured open water forces. The deviations in % are displayed in Figures 23 – 25, where

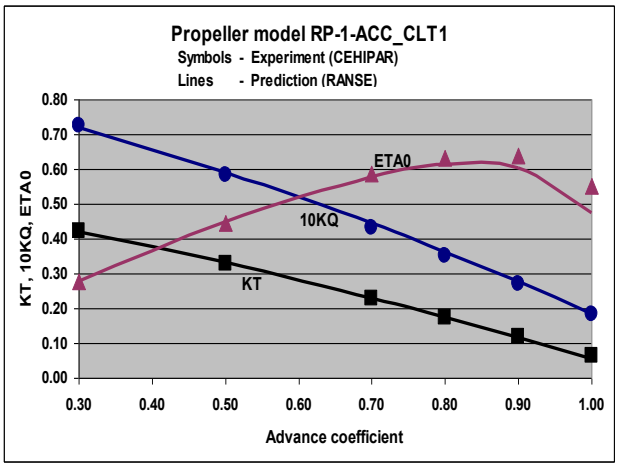

Figure22: Open water characteristics of the propulsor.Grid3

the grid convergence can also be observed.

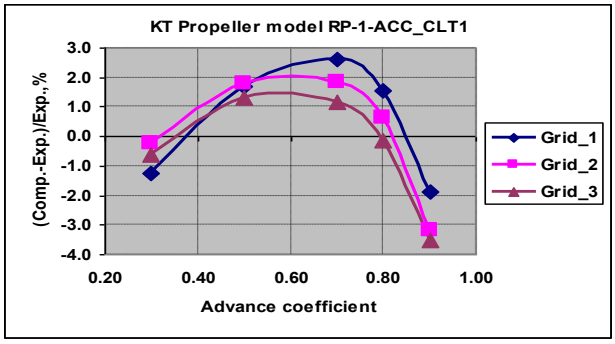

Figure 23: Validation of model open water thrust coefficient

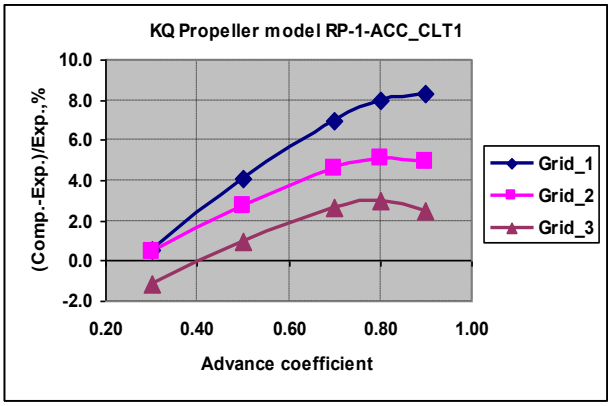

Figure 24: Validation of model open water torque coefficient.

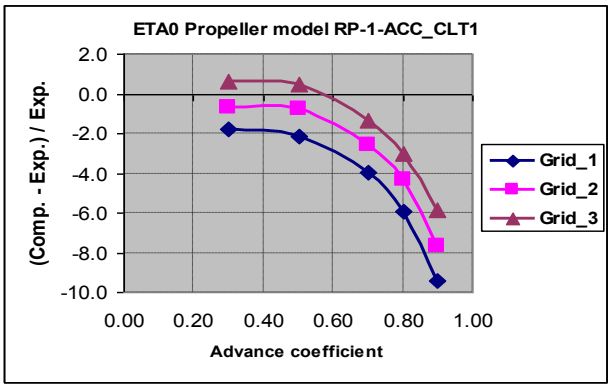

Figure 25: Validation of model open water efficiency.

When the turbulence model from *SST* was set to k-ε, the relative difference of the forces was found inside 3%, favourable to the SST model.

The contribution of the plate to the total thrust and torque of the propeller model can be observed in Figure 26.

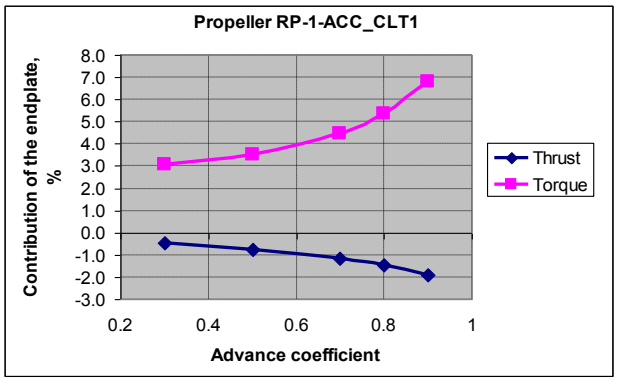

Figure 26: Contribution of the endplate to total forces.

4.2 Scale effect for the CLT propeller

The real full scale geometry of the propeller of the ship was used for open water computations. The angular velocity of the propeller was extrapolated by Froude similarity. The corresponding Reynolds number varies with the advance ratio in the range 6.8E+07 to 7.4E+07. The rest of the parameters have been kept constant.

The RANSE results for the forces and the efficiency are presented as relative deviation $\Delta K = (K_S - K_M)/K_M$ of the full (ship) from the model scale and shown in Figure 27.

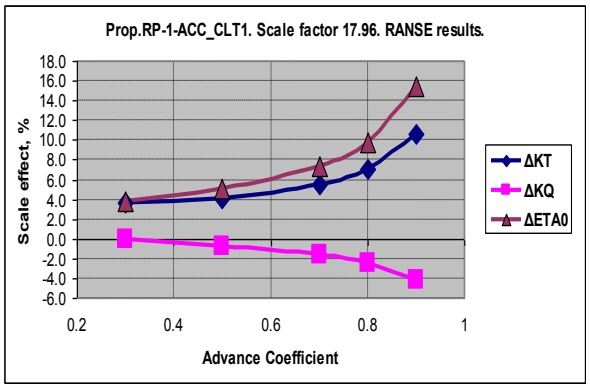

Figure 27: Scale effect on open water of CLT propeller.

The computational results are compared to the extrapolation method for CLT propellers used actually in practice and described in Pérez Sobrino et al (2005). The comparison for advance coefficient corresponding to the design point of the propeller is shown in Figure 28.

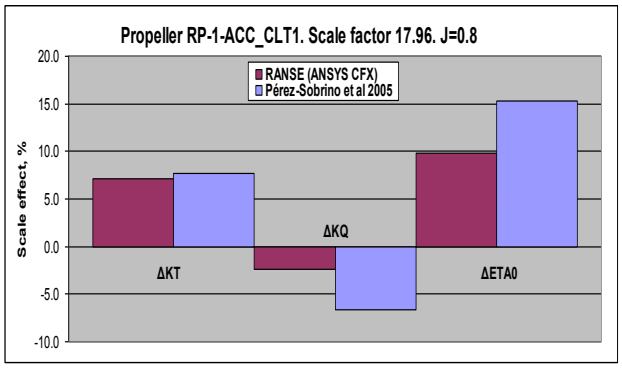

Figure 28: Comparison of calculated open water scale effect.

4.3 Discussion

As can be seen from the results shown in Figures 22 – 25, the computed thrust and torque of the CLT propeller in uniform flow compare favourably with model open water measurements, at least for moderate and high loading conditions. The torque, and consequently, the efficiency are affected more by the grid size than the thrust. The contribution of the endplate to the total forces (Figure 26) increases with the advance ratio and is higher for the torque. The plate has minor negative contribution in full than in model scale, all this confirming the results Sánchez-Caja et al (2006) obtained for CLT propeller of different geometry.

In the frames of the present approach, the scale effect on the forces (Figure 27) increases with the advance ratio and reaches values higher than usually estimated for the conventional propellers. The numerical results show that the gain of efficiency in full scale, as also observed for conventional propellers, is due to the simultaneous increase of the thrust and decrease of the torque, but with the former being more pronounced than the latter. The higher contribution of the thrust is also observed in Sánchez-Caja et al (2006) but the comparison warns that the extrapolation tendency of the components may depend on the characteristics of the blades and the endplate, and on the difference of the flow conditions at model and full scale.

As can be observed in the comparative Figure 28, the RANSE code predicts lower scale effect for the torque and the efficiency than the procedure adopted actually for extrapolation of open water results of CLT propellers.

5 CONCLUSIONS

The commercial RANSE code ANSYS CFX and the meshing tool ICEM have been successfully implemented for the computation of the open water performance of ducted and CLT endplate propellers. The validation with model tests permitted establishing the mesh resolution necessary to obtain acceptable precision of the predictions for the cases treated in the present study. A typical simulation timescale of 0.01 seconds was adopted. The number of iterations depends on the loading conditions and did not exceed 500 to achieve the convergence precision criteria of 10^{-4} for the maximum of residuals. The computations have been carried out on 64 bits AMD "Opteron 250" computer of 16 GB main storage. The typical computer time for one advance is about 5 hours.

The forces at model scale have been satisfactorily predicted, as demonstrated by comparison with open water test results. For controllable pitch propellers having high hub ratios, the prediction set up should distinguish between open water and self propulsion test arrangements for correct comparison.

The scale effect has also been approached and useful conclusions have been drawn, but this study does not pretend to give practical data nor recommendations for extrapolation from model to full scale, as not all the parameters involved in the scaling have been taken into account.

For ducted propellers, the convergence of the forces with the resolution of the mesh was found less pronounced than for free-running and CLT ones. The computations show that for moderate loadings, the total thrust is almost not affected by the scale and this may be associated not only to the behaviour of its components, but also with the range of Reynolds number, being all model values above $5*10^4$ (Hoekstra 2006), (Zondervan et al 2006). Nevertheless, in the present approximation, the scale effect on the torque is not negligible and may differ from the effect observed for free running propellers.

Concerning the CLT propellers, it has been shown that the RANSE code prediction of the model open water curves is reliable and the precision is not less than the obtained for conventional propellers. Although the computational effort is still quite high for a practical design, as we know, this unique approach is able to simulate the forces on endplate propellers with satisfactory precision. The claim for considerable scale effect suffered by this particular CLT propeller has been confirmed by the computational results. Certainly, one or two cases are not sufficient to draw more general conclusions for the extrapolation from model to full scale and further research is necessary, but

there is no doubt that the viscous flow analysis can contribute to this goal.

This study also indicates the need for new benchmark experiments of flow details measurements to further validate the computations for both types of propulsors.

ACKNOWLEDGEMENTS

This work was supported by the European Commission, FP7 Collaborative Project, nº234182 (SILENV) and by CEHIPAR.

The authors gratefully acknowledge Mr. Antonio Fabuel for generating quality CAD models of the propulsors. The review by Dr. Amadeo García is also acknowledged.

Thanks are due to Dr. Jose Falcao de Campos (IST), Dr. Johan Bosschers (MARIN) and Mr. Juan González-Adalid (SISTEMAR) for kindly offering the detailed input data and test arrangements and for the comments.

NOMENCLATURE

c	LCH	Chord length
C_p	CP	Pressure coefficient on axial speed V_∞ $= 2(p-p_\infty)/(\rho V_\infty^2)$
C_{Th}	CTH	Thrust loading coefficient
J	JEI	Propeller advance coefficient
K_{COMP}		Computed force coefficient
K_{EXP}		Experimental force coefficient
K_{TD}	KTD	Duct (nozzle) thrust coefficient
K_{TP}	KTP or KT	Propeller thrust coefficient
K_{TT}	KTT	Total thrust coefficient (KTP+KTD)
K_Q	KQ	Propeller torque coefficient
L_D	LD	Duct length
n	FR	Propeller frequency of revolution
Rn_D	RND	Reynolds number of nozzle: $V_\infty * L_D / \nu$
Rn_P	RNP	Reynolds number of propeller: $c_{0.7Rp} * \sqrt{V_\infty^2 + (1.4\pi n R_p)^2} / \nu$
R_p	RP	Radius of the propeller (DP/2)
V_∞	VA	Propeller advance speed
s		Chordwise coordinate on duct (0 – LE, 1 – TE)
ν	VK	Kinematic viscosity
η_0	ETA0	Open water efficiency
ρ	RHO	Mass density of water
τ	TMR	Thrust ratio (propeller to total thrust)

REFERENCES

Abdel-Maksoud, M. & Heinke, H.-J. (2002). 'Scale Effects on Ducted Propellers'. Proceedings of the 24th Symposium on Naval Hydrodynamics, Fukuoka, Japan.

ANSYS CFX v.12 (2009). Documentation.

Baltazar, J. & Falcao de Campos, J. A. C. (2009). 'On the modelling of the flow in ducted propellers with a panel method'. Proceedings of the First International Symposium on Marine Propellers, Trondheim, Norway.

Bobo M. J., De La Rosa J.-C., Masip J., Quereda R. & Pangusión, L. (2005). 'Design of ducted propeller and model tests of a fishing research vessel for M.Cies Shipyards'. OTI 2233-2, CEHIPAR (in Spanish).

Falcao de Campos, J. A. C. (1983). On the calculation of ducted propeller performance in axisymmetric flows. PhD Thesis, Delft University, Wageningen, The Netherlands.

Gennaro, G., González-Adalid, J. & Folso, R. (2009). 'Contracted and loaded tip (CLT) propellers: Latest installations and experiences'. Proceedings of the 16th International Conference of Ships and Shipping Research (NAV2009), Messina**,** Italy.

Haimov, H., Terceño, M. & Trejo, I. (2007). 'Use of Commercial RANSE Code for Open Water Propeller Calculations'. Proceedings of 10th NuTTS, Hamburg, Germany.

Haimov, H., Bobo, M.J., Vicario, J. & Del Corral, J. (2010). 'Ducted propellers. A Solution for Better Propulsion of Ships. Calculations and Practice'. Proceedings of First International Symposium on Fishing Vessel Energy Efficiency, Vigo, Spain.

Hoekstra, M. (2006). 'A RANS-based analysis tool for ducted propeller systems in open water conditions'. International Shipbuilding Progress **53**, pp.205-227.

Kinnas, S. A., Chang, S.-H., Yu, Y.-H. & He, L. (2009). 'A Hybrid Viscous/Potential Flow Method for Prediction of the Performance of Podded and Ducted Propellers'. Proceedings of Propeller/Shafting'09 Symposium, SNAME, Virginia Beach, United States.

Krasilnikov, V., Sun, J., Zhang, Z. & Hong, F. (2007). Mesh Generation Technique for the Analysis of Ducted Propellers Using a Commercial RANSE Solver and its Application to Scale Effect Study'. Proceedings of 10th NuTTS, Hamburg, Germany.

Kuiper, G. (1992). 'The Wageningen Propeller Series'. MARIN **92-001**.

Pérez Gómez, G. & González-Adalid, J. (1995). 'Tip Loaded Propellers (CLT). Justification of their advantages over conventional propellers using the momentum theory'. International Shipbuilding Progress **429**, pp. 5-60.

Pérez Sobrino, M., Minguito Cardeña, E., García Gómez, A., Masip Hidalgo, J., Quereda Laviña, R., Pangusion, L., Pérez Gómez, G. & González-Adalid, J. (2005). 'Scale Effects in Model Tests with CLT Propellers'. Proceedings of 27th Motor Ship Marine Propulsion Conference, Bilbao, Spain.

Sánchez-Caja, A., Rautaheimo, P. & Siikonen, T. (2001). 'Simulation of Incompressible Viscous Flow Around a Ducted propeller Using a RANS Equation Solver'. Proceedings of 23rd Symposium on Naval Hydrodynamics, Val de Reuil, France.

Sánchez-Caja, A., Sipilä, T. & Pylkkänen, J. (2006). 'Simulation of the Incompressible Viscous Flow around an Endplate Propeller Using a RANSE Solver'. Proceedings of 26th Symposium on Naval Hydrodynamics, Rome, Italy.

Zondervan, G-J., Hoekstra, M. & Holtrop, J. (2006). 'Flow Analysis, Design and Testing of Ducted Propellers'. Proceedings of Propeller/Shafting Symposium, Virginia Beach, United States.